Optical and electrical resistivity studies of isovalent and aliovalent 3*d* transition metal ion doped ZnO

Shubra Singh and M. S. Ramachandra Rao
Department of Physics, Materials Science Research Centre and Nanofunctional Materials Technology Centre, Indian Institute of Technology Madras, Chennai 600 036, India
(Received 5 May 2009; revised manuscript received 18 June 2009; published 30 July 2009)

In this paper, we report on the optical and electrical transport studies of TM ion (Ni, Ti, V, Fe, Cr, Mn, and Co) doped ZnO polycrystalline samples. Diffuse reflectance spectroscopy of doped ZnO showed the existence of absorption bands which were attributed to the *d-d* transitions of respective dopants. Electrical resistivity was found to decrease in case of Ti-, V-, Fe-, and Ni-doped ZnO bulk samples as compared to undoped. We explain the above behavior on the basis of impurity *d*-band splitting model. It is observed that with increase in dopant content the temperature range where variable-range hopping is valid shrinks to lower values and the activation energy lowers. Increase in characteristic temperature and decrease in localization length was observed with increase in TM ion content pointing towards the delocalization of electrons that sets in with doping.

DOI: 10.1103/PhysRevB.80.045210 PACS number(s): 72.80.Ey, 61.72.uj

I. INTRODUCTION

ZnO which occurs naturally as the mineral zincite, finds a wide range of applications in varistors, pigments, UV protection lotions, magneto-optic, and spintronic devices. Highly crystalline bulk ZnO presents possibilities for short-wavelength (blue/UV) light-emitting diodes, laser, magneto-optic, and optoelectronic applications. The interest in determining electrical transport and optical properties of doped bulk ZnO has motivated us because of the need to develop an understanding of the material response to impurities introduced by doping.[1]

ZnO is a direct wideband-gap semiconductor and can be readily made into an *n*-type degenerate semiconductor with high dielectric constant ($\sim$10) and exhibits activated conduction.[2] Realization of diluted magnetic semiconductor (DMS) behavior in such wideband-gap materials provide an important insight into spin injection applications as in spin filters and spin transport media. There has been an intense search for inherent wideband-gap-oxide-based DMS systems ever since the theoretical prediction of Dietl.[3] ZnO normally crystallizes in hexagonal wurtzite crystal structure with a=3.25 Å and c=5.12 Å, and a c/a ratio=1.6. In ZnO, the Zn atoms are tetrahedrally coordinated to four oxygen atoms, where Zn 3*d* electrons hybridize with the oxygen 3*p* electrons. Addition of impurities to ZnO lattice often induces dramatic changes in the physical properties. Doping ZnO lattice with Ga or Al increases the carrier density [$\sim 10^{20}$–10^{21} cm^{-3}] compared to undoped [$\sim 10^{17}$–10^{18} cm^{-3}] ZnO (Refs. 4 and 5). Nanophased ZnO phases doped or alloyed with Ga,[6,7] Ni,[8] Cd,[9] and Mg,[10] have also been reported. There has been a great deal of focus on search for magnetism in transition metal ion (TM) doped ZnO.[11–14] Theoretical calculations predict that for V-, Cr-, Fe-, Co-, or Ni-doped ZnO, ferromagnetic state is stable without the need for any additional carrier-doping treatment.[15]

Despite its technological importance, the electrical property of TM ion doped ZnO is not well understood and the resistivity behavior of bulk TM ion doped ZnO needs to be investigated systematically. In our recent work[16] on transport property of Ni-doped ZnO, we showed a significant decrease in resistivity of the Ni-doped ZnO with very small Ni concentrations (1 and 2 mol %). We explained this decrease in the bulk resistivity of Ni-doped ZnO based on the impurity *d*-band splitting model invoking Katayama's *ab initio* calculations on doped GaN- and ZnO-based systems.[17,36] This result has motivated us to investigate further the influence of other transition metal ions, namely, Cr, Mn, V, Fe, Co and Ti dopants on the transport and optical properties of ZnO (bulk and thin film). In this study, we systematically studied the electrical resistivity of doped ZnO compounds in bulk and thin-film form and correlated the results with optical and Raman data. Attempts were made to study the room-temperature magnetic nature of the samples. All these results are presented in the following sections to elucidate the optical and electrical properties of doped ZnO systems and to find if magnetism exists in this wideband-gap material.

II. EXPERIMENTAL DETAILS

High pure ZnO and oxides/carbonates of transition metals were used to prepare bulk $Zn_{1-x}TM_xO$ (x=dopant concentration and TM=transition metal ion) by conventional sol-gel technique. Sol-gel technique was used in order to realize good homogeneity and atomic-scale mixing of ingredients. The chemical ingredients were weighed in stoichiometric proportions and dissolved in about 40 ml of deionized water, and stirred continuously using a magnetic stirrer. After about an hour of stirring, proportionate weight of citric acid was added and the resulting solution was almost clear. However, to make it completely transparent, a few drops ($\sim$3 ml) of HNO_3 were added. The resulting solution was again stirred for about 2 h. The temperature of the solution was slowly raised in small steps (5 °C after every 2 h). After the formation of gel, the temperature was further raised to 100 °C so that the water in it completely boiled off. The resultant powder was heated first at 600 °C for 24 h and then again at 900 °C for 24 h, with intermittent grindings, to completely remove water vapor, citrate, and nitrate impurities. The pow-

der was then made into disk-shaped pellets (~8 mm diameter and ~2 mm thickness) by uniaxial pressing. In order to densify the targets, the disklike specimens were sintered at 1200 °C for 24 h. Thin films of the above samples were grown on Si (100) substrates by pulsed laser deposition (PLD) at a substrate temperature of 500 °C and at an oxygen partial pressure of 5×10^{-5} mbar.

The phase purity of ZnO and TM ion doped ZnO was studied by x-ray diffractometer (PAN analytical Xpert-Pro-PHILIPS) using Cu $K\alpha_1$ radiation ($\lambda = 1.5405$ Å). The other characterization studies involves were scanning electron microscopy (PHILIPS, QUANTA-200), diffuse reflectance spectroscopy (Ocean optics USB 2000 spectrophotometer), photoluminescence [Spectro fluorometer (Jobin Yvon)], Raman spectroscopy (Jobin Yvon), and electrical resistivity (linear four-probe method). For photoluminescence measurements the samples were excited at a wavelength of 325 nm at room temperature. Diffuse reflectance spectra (DRS) of homogenized powder samples were recorded using an Ocean Optics UV-VIS-NIR spectrometer by collecting scattered light from powdered samples. These spectra were recorded using a $BaSO_4$ powder compact (white in color) used as a reference sample. Raman-scattering measurements on the bulk samples were performed using He-Ne laser (632.8 nm) at room temperature. The resolution used in Raman measurements is 0.1 cm^{-1}.

Room-temperature and low-temperature magnetic measurements were carried out using superconducting quantum interference device (SQUID) magnetometer and vibrating sample magnetometer (VSM).

III. RESULTS AND DISCUSSION

A. Bulk undoped and doped ZnO samples

The solid solubility limit of TM ions in ZnO is found to be dopant specific and to some extent depends also on the preparation technique. For example, the solubility limit of Ni in bulk ZnO has been reported as 3 mol %.[18] However, under our preparative conditions, impurity peaks of NiO were observed for 2.5 mol % of Ni-doped ZnO.[16] The valence states of doped ions can be ascertained using DRS, where the transitions between impurity states appear as midband-gap absorption states. Ni-doped ZnO samples showed the existence of *d-d* transition band states at 430, 580, and 655 nm which are characteristic of Ni (II) with tetrahedral symmetry.

We observed a decrease in resistivity, by about 2 orders, in Ni-doped (1 and 2 mol %) bulk polycrystalline ZnO samples.[16] The decrease in resistivity was found to be in accordance with the impurity *d*-band splitting model of Katayama *et al.*[17] As shown by this model (Fig. 1), the splitting of *d* levels under the influence of a crystal-field leaves the antibonding states close to this conduction band (CB), thus facilitating an increase in conduction, as carriers can be transported into the CB with great ease. *Ab initio* electronic-structure calculations[17] showed that a half-metallic behavior is expected for V-, Fe-, Co-, and Ni-doped ZnO. The magnetic impurity *d* states in DMS, generally appear near the Fermi level (here TM ion is the magnetic impurity in ZnO). These states exhibit splitting, resulting in the high-spin con-

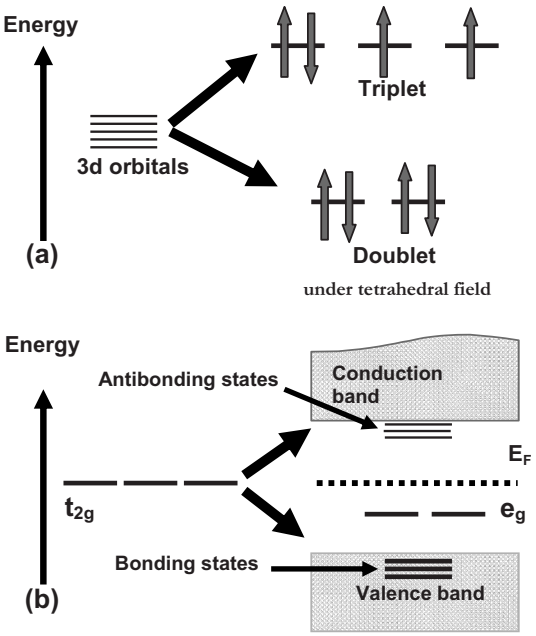

FIG. 1. Depiction of a model to understand the changes in electronic structure in the case of transition metal ion doping at a substitutional site in a wurtzite structure. (a). Crystal-field effect of ZnO on 3*d* metal ion leading to doublet and triplet formation and (b) Impurity states split under the influence of crystal field of the host (ZnO in this case).

figuration of *d* electrons and the impurity states undergo hybridization with valence *p* states of the host compound. For phase pure samples, TM ion replaces the Zn^{2+} ion which is at the center of the tetrahedron. The *d* states of a TM ion split under the influence of the tetrahedral crystal field of ZnO, leading to lower doublet e_g state and a higher-energy triplet t_{2g} state. The t_{2g} states hybridize with the *p* orbitals of the valence band further splitting into t_{bonding} and $t_{\text{antiboding}}$ states. The t_{bonding} states participate in bonding and hence are localized. The antibonding states have higher energy and contain itinerant electrons. The energy of the bonding states lie close to the conduction band of ZnO and hence with the increase in temperature, electrons in this state can jump easily in to the conduction band because of thermal activation. However, the amount of splitting leading to the proximity or overlapping of antibonding states with the CB may differ for each dopant ion. This study was further extended to other 3*d* transition metal ions, namely, Cr, Mn, V, Fe, Co, and Ti.

B. XRD studies of bulk undoped and doped samples

Figure 2) shows XRD patterns of doped and undoped bulk ZnO. We found that under our preparative conditions, the solubility limits of Cr, Mn, V, Fe, Co, Ni, and Ti in bulk ZnO were 1 mol %, 3 mol %, 2 mol %, 1 mol %, 5 mol %, 2 mol %, and 2 mol %, respectively. Impurity peaks of respective oxides were observed for higher values of doping in each case. Thus for the sake of uniformity, we restricted our study to single-phase compounds of 1 mol% doped ZnO and the results presented herein pertain to 1 mol% of dopant ion in ZnO. The dopant percentage is within the solubility limit

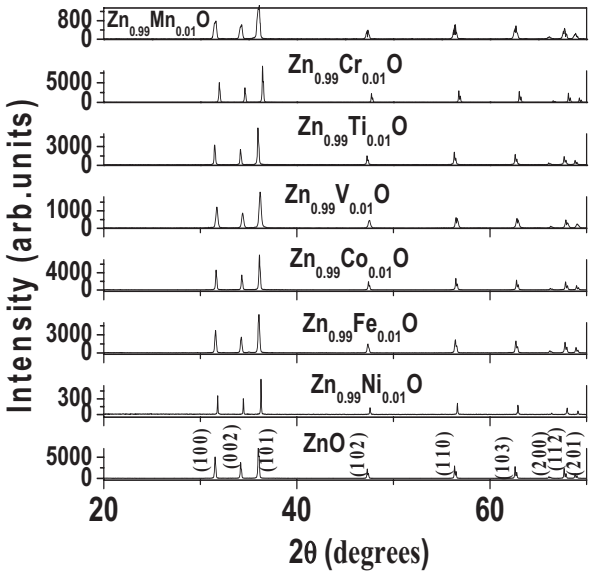

FIG. 2. XRD patterns of bulk undoped and 1 mol% Ni-, Fe-, Co-, V-, Ti-, Cr-, and Mn-doped ZnO samples.

in each case. Besides this, in the present preparation technique, as atomic level mixing is expected in materials prepared by sol-gel technique, upon subsequent we expect the metal ions to be incorporated in substitutional sites replacing the Zn^{2+} ion and not precipitate out as secondary entities. This view was further corroborated by the optical studies performed on the doped samples.

C. DRS

DRS measurements on powder samples or pellets are roughly analogous to transmission measurements on thin films.[19] Figure 3 shows diffuse reflectance spectra of ZnO and transition metal ion doped ZnO bulk samples. Undoped ZnO sample showed the absorption edge around 380 nm. Doped ZnO samples exhibited absorption peaks in the visible region in addition to the absorption edge since the samples containing TM ions will have bands from crystal-field transitions of ions in tetrahedral coordination. These absorption peaks in the visible region are attributed to various transition metal ions substituted at the Zn site. In the case of Co-doped ZnO, the absorption peaks are well separated from absorption edge and absorption peaks at 612 and 568 nm are attributed to the presence of Co^{2+} in ZnO lattice. These absorption peaks are expected to arise due to electronic transitions from the $^4A_2$ ground state to the $^4T_1(P)$ state for the tetrahedral Co (II). The two sharp absorption peaks of Co-doped ZnO are assigned as $^4A_2(F) \rightarrow {}^4T_1(P)$ (612 nm) and $^4A_2(F) \rightarrow {}^2A_1(G)$ (568 nm).[20] These *d-d* transitions indicate that Co is in the divalent state at the Zn site with its high-spin electron configuration.

Absorption spectrum of Ni^{2+}-doped ZnO shows the midband-gap states appearing at about 430, 580, and 655 nm, corresponding to the *d-d* transition bands, which are characteristic of Ni (II) with tetrahedral symmetry.[21] The absorption around 655 nm corresponds to the $^3T_1(F) \rightarrow {}^3T_1(P)$ ligand field transition of Ni^{2+} ions in tetrahedral symmetry.

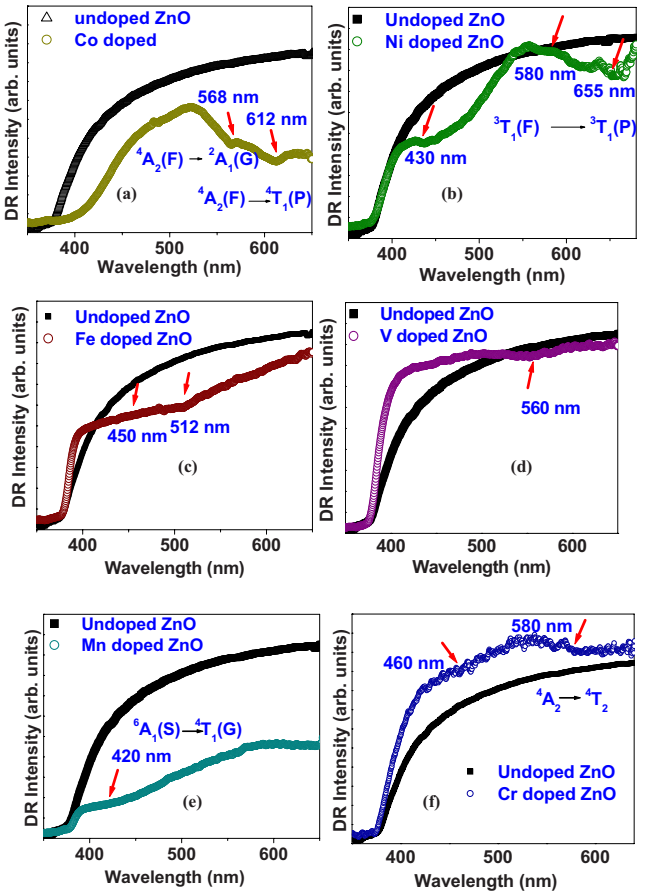

FIG. 3. (Color online) Diffuse reflectance spectra of bulk polycrystalline undoped and Co-, Ni-, Fe-, V-, Mn-, and Cr-doped ZnO sample. Absorption peaks corresponding to dopant absorption states are clearly indicative of dopant incorporation and formation of midband-gap states.

Similarly, for Fe-doped ZnO samples, absorption band at 450 nm has been attributed to Fe^{3+} in tetrahedral co-ordination.[22] Grygar *et al.*[23] reported that, for Fe-doped ZnO, the absorption at 512 nm can be attributed to some form of tetrahedrally or octahedrally coordinated Fe(III) ions. No significant absorption corresponding to Fe^{2+} ions were observed and hence determination of the presence of tetrahedral Fe^{2+} by optical spectra was not possible.

For V-doped samples the absorption around 560 nm represents typical *d-d* transition of V^{2+} ions in a tetragonal crystal field.[24] For Mn-doped ZnO, the broad absorption peak centered around 420 nm is assigned to $^6A_1(S) \rightarrow {}^4T_1(G)$ transition.[25] The midband-gap states arising due to absorption at 460 and 580 nm correspond to the *d-d* transition bands of Cr ions. The broad absorption band around 580 nm corresponds to the $^4A_2 \rightarrow {}^4T_2$ transition.[26] However, for Ti-doped ZnO sample the absorption around 600 nm could not be attributed to *d-d* transitions of Ti ion and further studies are needed to get an idea of valence state of Ti ion in the parent ZnO phase.

D. Photoluminescence

Figure 4 shows the normalized room-temperature photoluminescence (PL) spectra of the bulk $Zn_{0.99}TM_{0.01}O$

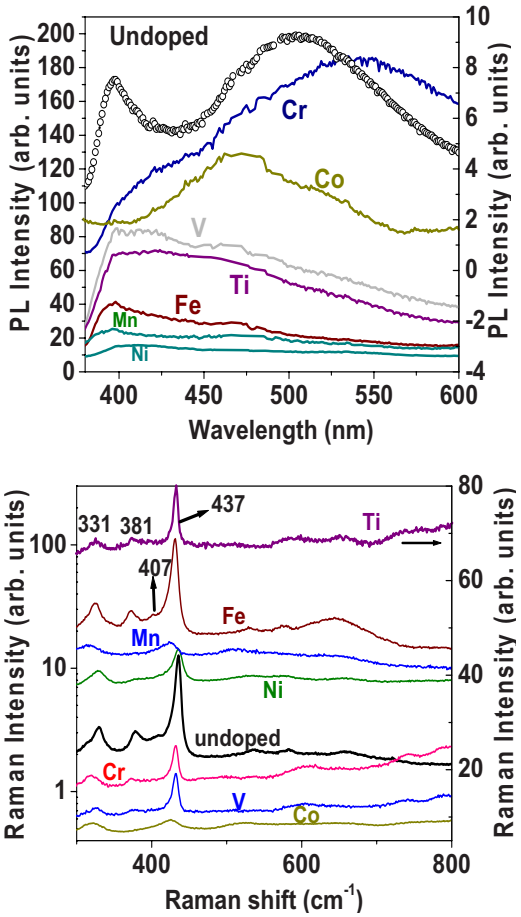

FIG. 4. (Color online) Normalized room-temperature PL spectra of the bulk $Zn_{0.99}TM_{0.01}O$ (TM=Transition metal ion) compounds. The spectra corresponding to TM ion doped compounds have been marked, respectively, by the dopant elements. Excitonic emission is suppressed in doped compounds as compared to the undoped ZnO. The different plots have been shifted vertically to show the different peaks for each dopant.

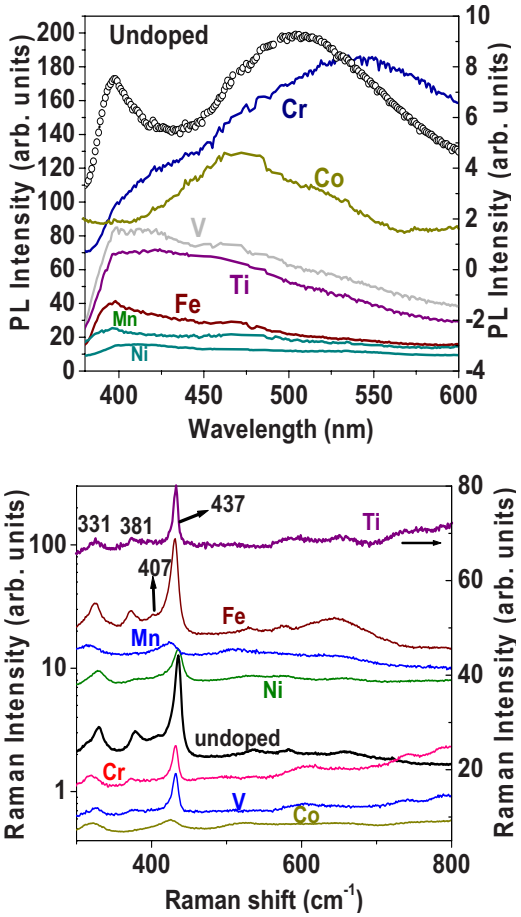

FIG. 5. (Color online) Normalized room-temperature Raman spectra of the bulk $Zn_{0.99}TM_{0.01}O$ compounds. The different plots have been shifted vertically to show the different peaks for each dopant.

samples. Compared with the undoped ZnO sample, the excitonic emission is suppressed in doped compounds, which indicates that the TM ion doping increases the nonradiative recombination processes. The TM ions are expected to act as killer centers to suppress the transitions resulting in radiative recombination. These nonradiative transitions may arise when free electrons recombine via a TM ion impurity level instead of populating donor-acceptor pairs and can also be attributed to energy-transfer processes from donor-acceptor pairs to neighboring TM ions.[27,28] Efficiency of nonradiative recombination process depends on relative concentration of different species involved, their carrier-trapping rates and also the ionization cross section of TM ion which is different for each TM ion and also the host.[27,28]

E. Raman spectra

A precise knowledge of the vibrational modes can give us a fundamental understanding of the electrical and thermal properties of a single crystal. In wurtzite ZnO (number of atoms per unit cell being 4), the total number of phonon modes are 12, namely, one longitudinal-acoustic (LA), two transverse-acoustic, three longitudinal-optical (LO), and four transverse-optical (TO) branches. The active Raman modes include A_1, E_1, and the two nonpolar E_2 branches. The A_1 and E_1 modes are each split into LO and TO components with different frequencies due to macroscopic electric fields associated with the LO phonons. For the lattice vibrations with A_1 and E_1 symmetries, the atoms move parallel and perpendicular to the c axis, respectively. The vibration of heavy Zn sublattice gives rise to the low-frequency E_2 mode while that of oxygen sublattice gives rise to high-frequency E_2 mode. The modes E_1(TO) and A_1(TO) reflect the strength of the polar lattice bonds.

Lu *et al.* and Ashkenov *et al.*[29,30] reported the phonon modes in PLD deposited ZnO thin films. The nature of the different Raman modes occurring in ZnO have been reported in detail before.[31,32] Manjón *et al.*[33] compared the experimental results with the reported *ab initio* calculations of the lattice dynamics in wurtzite ZnO. In various reports occurrence of additional lines were observed at 205, 331, and 539 cm^{-1}[34–35] and were reported to be due to second-order Raman spectra. Raman spectra of as prepared undoped and doped samples are shown in Fig. 5. We observe the presence of peaks at 663 (A_1(LO)+E_2(low)), 538 cm^{-1} (2LA mode),

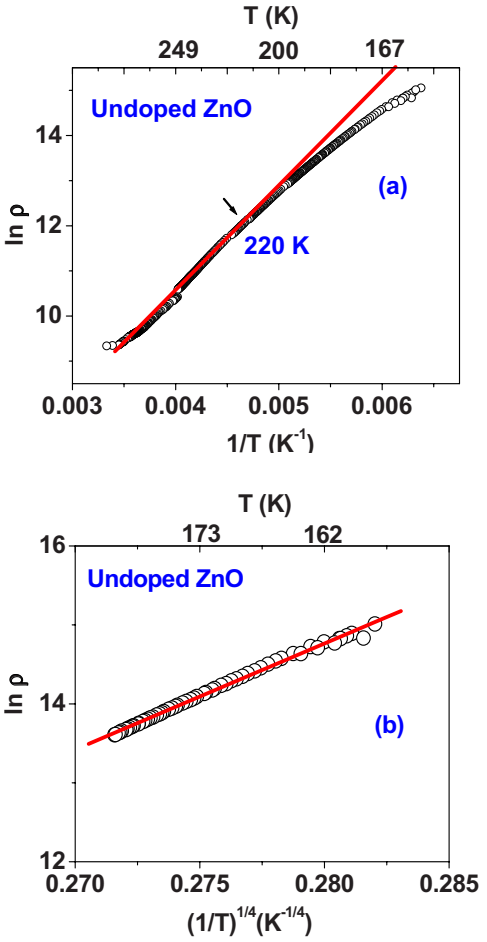

FIG. 6. (Color online) Curve fits (solid line) to the experimental data points (open circles) fitted to (a) resistivity with the thermal-activated model $\rho(T)=\rho_o \exp(\Delta E/k_B T)$; (b) resistivity with the variable-range-hopping model.

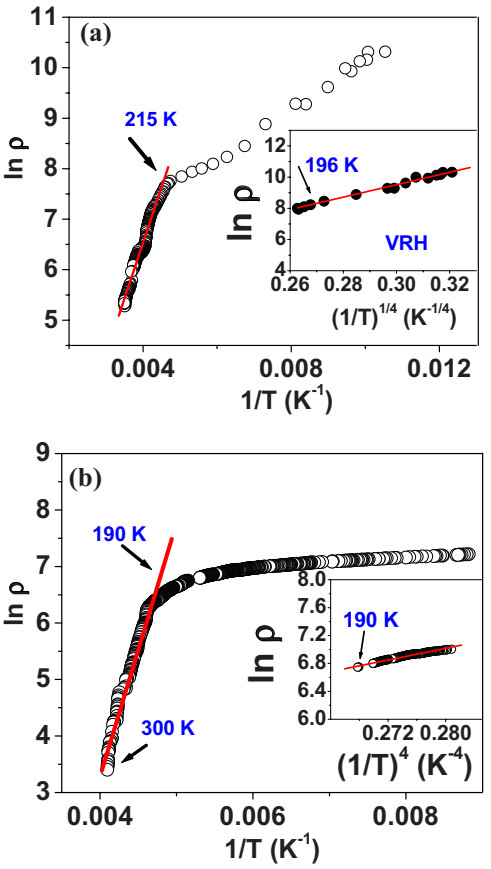

FIG. 7. (Color online) Curve fit of experimental data for resistivity with the thermal-activated model $\rho(T)=\rho_0 \exp(\Delta E/k_B T)$ for (a) 1 mol % (b) 2 mol % Ni doping. Inset shows curve fit of experimental data for resistivity that fit to the variable-range-hopping model.

437 cm^{-1} (attributed to nonpolar optical phonon E_2 mode of ZnO), 407 cm^{-1} [E_1(TO) mode], and 381 cm^{-1} [A_1(TO) mode] for undoped ZnO. The peak at 331 cm^{-1} can be attributed to single crystalline nature of ZnO (Refs. 34–36) and corresponds to the $E2(\text{high})-E2(\text{low})$.[31]

The peak at 583 cm^{-1} belongs to E_1 LO mode for undoped ZnO sample. In the Co-doped sample, only three peaks at 331 cm^{-1}, 437 cm^{-1}, and 538 cm^{-1} are prominently seen, however they are found to shift to lower frequency compared to undoped compound. For V-, Ni-, Ti-, and Fe-doped ZnO samples all the Raman frequencies are shifted toward the low-frequency side. Such a shift is expected to depend on residual stress, structural disorder, and crystal defects present in the samples. The lattice defects and disorder disrupts the long-range ordering in ZnO and weakens the electric field associated with a mode. For V doping, the 579 cm^{-1} mode seems to merge with a mode at 609 cm^{-1}. An additional mode appears at 744 cm^{-1} for this doping level. Such additional modes are also referred to as anomalous modes (AMs). AM for the Fe-doped sample occurs at 626 cm^{-1}. Anomalous modes at 274, 598, 641.9, and 857 cm^{-1} in Raman spectra of N-doped ZnO were reported by Kaschner *et al.*[37] who ascribed them to nitrogen-induced local vibrational modes (LVMs). However, Bundesmann *et al.*[38] later observed that the same additional modes also emerged in the Raman spectra of Fe-, Sb-, Al-, and Ga-doped ZnO films, which suggested the LVMs originate from the intrinsic host-lattice defects. Ye *et al.*[39] studied two possible mechanisms to delineate the origin of anomalous modes: disorder-activated Raman scattering (DARS) or local lattice vibration. The DARS scattering is said to be induced by the breakdown of the translation symmetry of the lattice caused by defects or impurities due to the nature of the dopant or due to the growth conditions.[33] Therefore, it can be presumed that AMs in our samples could arise due to either of these two mechanisms.

TABLE I. Temperature ranges where Arrhenius and VRH mechanisms are satisfied.

Sample	Activated (K)	VRH (K)
Undoped	300–220	below 205
1 mol Ni	300–215	80–196
2 mol Ni	300–190	80–190

TABLE II. Activation energies of undoped and Ni-doped samples.

Sample	Activation energy (meV)
Undoped	270
1 mol Ni	180
2 mol Ni	170

F. Electrical resistivity

Electrical resistivity (ρ) plotted as a function of temperature for undoped ZnO (Ref. 16) showed a semiconducting behavior, where resistivity was found to increase with decrease in temperature and ultimately ρ became too large to be measured below 150 K. For doped ZnO phases, thermally activated band conduction has been found as the dominant mechanism at high-temperature region whereas in the low-temperature region, variable-range-hopping conduction is found to dominate. The thermal activation resistivity follows the following functional form:

$$\rho(T) = \rho_0 \exp(\Delta E/k_B T), \tag{1}$$

where k_B is the Boltzmann constant and ΔE is the activation energy. Equation (1) can be rewritten as $\ln \rho = \ln \rho_0 + (\Delta E/k_B)\cdot T^{-1}$. Figure 6(a) shows the curve fits to the experimental data points for resistivity of undoped ZnO with the thermal-activated model $\rho(T)=\rho_0 \exp(\Delta E/k_B)\cdot T^{-1}$ and Fig. 6(b) shows the fitting of resistivity of undoped ZnO with the variable-range-hopping (VRH) mechanism. From Fig. 6, we could see that in our samples, the electrical conductivity deviates from the linear Arrhenius behavior at temperatures below 220 K.

Figure 6(b) also indicates that the temperature dependence of resistivity of undoped ZnO follows three-dimensional (3D)-VRH more closely at temperatures below 220 K. ZnO compounds have been found to follow 3D-VRH in previous reports by Natsume and Bandyopadhyay *et al.*[2,40] The VRH mechanism is governed by $\rho(T) = \rho_o \exp(T_o/T)^{1/p}$, where ρ_o and T_o denote material parameters which do not (strongly) depend on temperature. The dimensionality is given by p and the fitting parameters are given by the following parameters:

$$\rho_o = (3e^2 \nu_{\rm ph})/\{8\pi[N(E_F)/\alpha k_B T]^{1/2}\} \tag{2}$$

and

TABLE III. The values of variable-range-hopping parameters obtained for a temperature of 150 K.

Sample (1 mol % doping)	Activation energy (meV)
Fe-doped ZnO	189
V-doped ZnO	20
Ti-doped ZnO	10

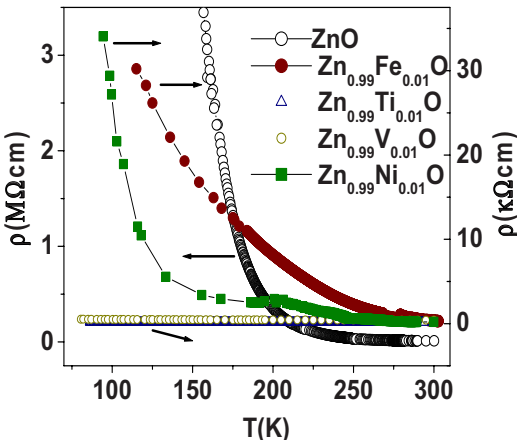

FIG. 8. (Color online) Electrical resistivity (ρ) vs temperature (t) of undoped and TM ion doped ZnO bulk samples. Cr-, Co-, and Mn-doped samples were found to be insulating, hence not included in the plot.

$$T_o = 16\ \alpha^3/[k_B N(E_F)], \tag{3}$$

where $\nu_{\rm ph}(\approx 10^{13}\ {\rm s}^{-1})$ is the phonon frequency at Debye temperature, k_B is Boltzmann's constant, $N(E_F)$ the density of localized electron states at Fermi level, and α the inverse localization length of the localized state.

The temperature variation in resistivity of bulk $Zn_{1-x}Ni_xO$ ($x=0.01$ and 0.02) (Ref. 16) shows that the samples are semiconducting in nature and the resistivity of doped samples decreases as dopant concentration increases. Figure 7 shows the curve fits of experimental data for resistivity with the thermal-activated model $\rho(T)=\rho_0 \exp(\Delta E/k_B T)$ and the variable-range-hopping model for Ni-doped samples. Tables I and II give an account of temperature range where Arrhenius and VRH mechanisms are satisfied and an account of the activation energies of undoped and Ni-doped samples. It is observed that with increase in dopant content, the temperature range where VRH is valid reduces to lower values and the activation energy lowers. The values of variable-range-hopping parameters for undoped and Ni-doped samples obtained for temperature of 150 K is given in Table III. The decrease in localization length with increase in Ni content points toward the delocalization of carriers that sets in with

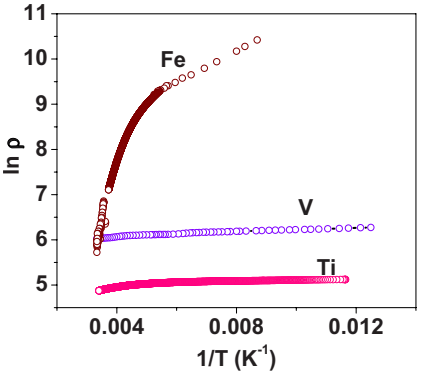

FIG. 9. (Color online) Simulation of experimental data for resistivity with the thermal-activated model $\rho(T)=\rho_o \exp(\Delta E/k_B T)$.

TABLE IV. Activation energies of doped ZnO samples.

Sample	T_o (K)	α (cm^{-1})	Localization length (cm)
Undoped	3.2×10^{8}	1.13×10^{5}	8.8×10^{-6}
1 mol Ni	2.54×10^{6}	1.81×10^{5}	5.5×10^{-6}
2 mol Ni	5.83×10^{5}	3.17×10^{5}	3.1×10^{-6}

Ni doping. The decrease in the localization length decreases the spatial extent of localized states. The observed smaller temperature range for Ni-doped ZnO film, in which VRH is applicable, is consistent with the smaller localization length found for the Ni-doped ZnO film. When this study was extended to other TM ion dopants, it was observed that Ti, V, and Fe doping decreases the resistivity of bulk ZnO as compared to the undoped ZnO (Fig. 8).[41]

The decrease in resistivity due to isovalent TM ion doping of V and Ni (valence state as confirmed from DRS studies) can be explained on the basis of band-splitting model as discussed in the Sec. I with respect to Ni-ion doping.[16] *Ab initio* studies on the TM ion doped ZnO compounds have also shown partial overlap of antibonding *d* states with the conduction band of host compound.[42] The itinerant electrons in these antibonding states can traverse to the conduction band and may be responsible for the observed decrease in resistivity of isovalent TM ion doped ZnO systems. However, in the case of Fe- and Ti-doped samples the presence of higher valence states cannot be completely ruled out. For example, the presence of Fe^{3+} ions in our samples was also corroborated by the DRS spectra. These ions are expected to give rise to donor defects, thereby making the sample more conducting. Ti also goes as Ti^{4+} ion and brings about extra carriers thereby lowering the resistivity.[43] Figure 9 shows the curve fits of experimental data for resistivity of Fe, Ti, and V with the thermal activated model $\rho(T)=\rho_0 \exp(\Delta E/k_B T)$ and Table IV lists the activation energies of doped ZnO samples. The values of variable-range-hopping parameters for Fe-doped sample obtained for $T=50$ K is given in Table IV and V, and Ti followed the Arrhenius behavior throughout the temperature range.

In case of other TM ion dopants, it was observed that the parent sample becomes more resistive upon doping Co, Cr, and Mn ions. Various other effects come into play in these doped systems, as summarized below: Badaeva *et al.*[44] employed the hybrid PBE1 calculations to show that the five Co^{2+} spin-up *d* electrons are delocalized in the VB of the ZnO cluster while the spin-down *d* electrons are localized just above the ZnO VB edges. Recent photoemission

TABLE V. Values of VRH parameters obtained for a temperature of 150 K.

Sample	T_o (K)	α (cm^{-1})	Localization length (cm)
ZnO	3.2×10^{8}	1.13×10^{5}	8.8×10^{-6}
1 mol % Fe	1.1×10^{6}	2.49×10^{5}	4×10^{-6}

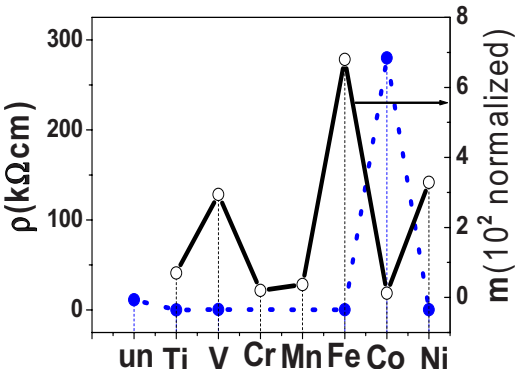

FIG. 10. (Color online) Comparison of room temperature ρ of TM ion doped ZnO bulk polycrystalline samples and room-temperature magnetic moment of TM ion doped ZnO bulk polycrystalline samples. Cr- and Mn-doped samples were insulating, hence their resistivity values have not been included in the plot.

studies[45,46] on bulk Co^{2+}-doped ZnO also show that pure $3d$ Co^{2+} states are located at the edge of the ZnO VB, well separated from conduction band which may be the reason for increase in resistivity of Co-doped samples.

The increase in resistivity of Co- and Mn-doped bulk samples can be attributed to the shallow acceptor nature of these impurities.[47,48] In such cases, the available electrons from the donor levels (the Zn interstitials and the oxygen vacancies) are trapped by the divalent ions, which results in the decrease in the *n*-type donor carrier concentration and therefore an increase in resistivity. On the other hand, Han *et al.*[49] calculated defect concentration and showed that Mn dissolved into ZnO forms a deep donor with an energy level of ~2.0 eV below the conduction-band bottom at room temperature. The existence of Mn deep donors depresses the concentration of the main shallow donor, thus increasing the resistivity. Increase in resistivity of Cr-doped samples can be attributed to the presence of Cr, which affects grain growth (well known as Cr poisoning) and decreases the carrier mobility due to carrier scattering at the grain boundaries.[50]

G. Magnetic measurements

Room-temperature ferromagnetism is the most sought after phenomenon in transition metal ion doped wideband-gap DMS compounds based on ZnO. In carrier-induced ferromagnetism, magnetic states are controllable by changing the carrier density.[42] There have been various conflicting reports on magnetism in TM ion doped ZnO samples.[13–15] The origin of ferromagnetism in oxides remains a very controversial topic. Many of the reports deal with the metallic clustering problem and secondary-phase formation leading to the occurrence of ferromagnetism.[51]

A few reports support the absence of magnetic clusters or secondary phases and support intrinsic ferromagnetic origin.[52] In order to investigate magnetism in our TM ion doped bulk samples, magnetic-moment studies were carried out using a Quantum Design SQUID magnetometer. It was found that parent ZnO, as expected, was diamagnetic while Ti-, V-, Ni-, Cr-, Co-, and Mn-doped samples were paramag-

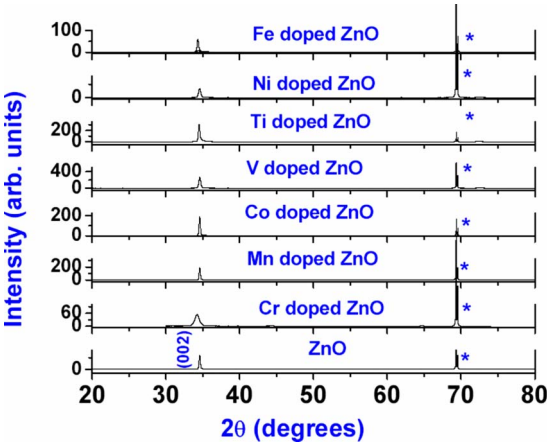

FIG. 11. (Color online) XRD patterns of undoped, Cr-, Mn-, Co-, V-, Ti-, Fe-, and Ni-doped ZnO thin-film samples. Peak marked with * corresponds to substrate (Si).

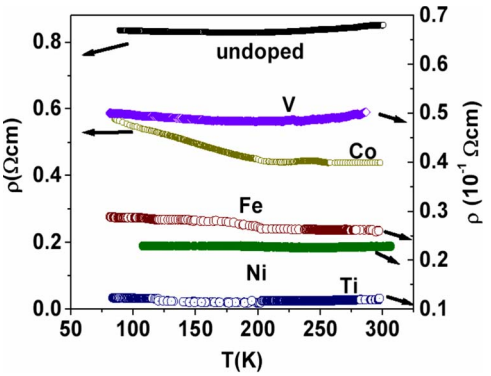

FIG. 12. (Color online) ρ (resistivity) vs T (temperature) of undoped and TM ion doped ZnO thin films. Cr- and Mn-doped thin-film samples were found to be insulating.

netic in the measured temperature range (5–500K). However, Fe-doped samples exhibited a cusp at 12 K indicating the presence of a Néel temperature and hence antiferromagnetism. To further confirm whether this behavior is due to intrinsic Fe doping or due to any impurity phase, we performed ^{57}Fe Mössbauer on these samples at room temperature. It was found that the sample showed a doublet splitting indicative of the presence of Fe in 3+ states in a cubic environment. This suggests that this behavior may be due the presence of minority $Zn_xFe_{3-x}O_4$ since Fe in ZnO is expected to be in a tetrahedral environment.

The magnetic-moment values have been obtained from the first quadrant of hysteresis loops for the respective samples and were normalized (μ_{3T}/μ_{0T} ratio of magnetic moment at 3 T and magnetic moment at 0 T recorded at room temperature) since the actual weights of the samples are not taken in to account. The bulk conducting samples of Ti, V, Fe, and Ni have magnetic moments ~0.7, 2.94, 6.8, and 3.29 (multiple of 10^2) which are much higher than the magnetic moments of 0.35, 0.37, and 0.2 (multiple of 10^2) for that of Co-, Mn-, and Cr-doped ZnO bulk samples (having higher resistivity than undoped sample). Though the parent compound becomes conducting on doping Ti, V, Fe, and Ni, yet no itinerant ferromagnetism was observed in all of the above cases. Figure 10 shows room temperature ρ of TM ion doped ZnO bulk polycrystalline samples and room-temperature magnetic moment of TM ion doped ZnO bulk polycrystalline samples. One interesting thing to be noted is that the samples with lower resistivity than doped compounds have higher magnetic moment and vice versa. The above aspect of our data is not clear and is under investigation.

H. Undoped and doped ZnO thin-film samples

The XRD profiles obtained on thin films (in Fig. 11) show single-phase-doped ZnO thin films with wurtzite structure. The films are epitaxial in nature with (002) peak appearing along with the substrate peak.

Figure 12 shows the electrical resistivity versus temperature plot for TM ion doped ZnO thin films. The films are found to be semiconducting in nature. Ti-, V-, Fe-, and Ni-doped ZnO samples are found to have lower resistivity than the undoped film, similar to the results obtained for their bulk counterparts. The room-temperature resistivity values of all samples, bulk as well as thin films, have been listed in Table VI.

The findings agree with some of the previous reports on the electrical resistivity of TM ion doped ZnO thin films. Shimono *et al.*[53] reported a decrease in resistivity [from 50 Ω cm for undoped to a value of 0.14 Ω cm for 2 mol % Ni-doped films] of Ni-doped ZnO thin film deposited by spin-coating technique. A report on *I-V* curve for Ni-doped ZnO nanowires showed a steep increase in conductance, indicating a great enhancement in conductivity by doping (ρ decreased from 390 Ω cm for undoped ZnO, to 12 Ω cm for doped films).[54] Our Ni-doped thin films showed consid-

TABLE VI. Comparison of ρ (resistivity) of doped and undoped ZnO samples at room temperature.

T (0 K)	Dopant	TM ion doped (1 mol %) doped bulk ZnO ρ(kΩ cm)	TM ion (1 mol%) doped ZnO thin film ρ(Ω cm)
300	undoped	11.34	8.5×10^{-1}
300	V	0.41	5×10^{-2}
300	Fe	0.23	2.6×10^{-2}
300	Co	Insulating	4.38×10^{-1}
300	Ti	0.14	1.2×10^{-2}
300	Ni	0.2	2.3×10^{-2}

erable decrease in resistivity from 8.5×10^{-1} Ω cm to 2.3×10^{-2} Ω cm. Electrical resistivity of ZnO films was also found to decrease from 4.14×10^{-3} Ω cm to 1.02×10^{-3} Ω cm after being doped with Ti.[55] Ti doping in ZnO has been shown to bring about changes in the electronic structure close to the conduction-band edge and Ti dopants were expected to act as donors.[56,57] Lin *et al.*[58] also reported the donor property of Ti dopants in ZnO. Contrary to the expectations, Co-doped ZnO thin films also showed a slight decrease in resistivity as compared to undoped ZnO (the possible reason for which is under investigation).

A VSM was used to determine the magnetic properties of TM ion doped thin films with the applied field perpendicular to the film plane. For Co-doped thin-film hysteresis loops were observed at 4 and 50 K, though in the presence of noise because of weak signal. The coercivity was measured to be about 100 Oe at 4 K. According to our experimental results, low-temperature hysteresis loops could be realized even for 1 mol% doped samples of Co-, Mn- and Fe-doped ZnO. However at higher temperatures the *M-H* curve did not show any sign of saturation. The source of magnetism of ZnO doped with Co at low concentration is still not totally understood. In our view, metal clusters may not be the source of magnetism at low Co concentration, as this concentration is well below the solid solubility limit of Co in ZnO. It is known that ferromagnetism is the usual explanation for hysteresis. However it is worth noting that spin glass and superparamagnetism below a blocking temperature can also be the cause of the hysteresis loop. An investigation of magnetization dependence on temperature can give us a clear idea of the exact nature of the magnetic behavior. However due to low signal (10^{-5}–10^{-6} emu) from the films the nature of *M-T* data obtained from VSM was very noisy. Therefore at this point, it is difficult to determine the nature of magnetization in our sample.

IV. CONCLUSION

We have systematically studied the electrical and optical property of TM ion doped ZnO. The presence of TM ions in the host lattice was confirmed through optical studies (DRS, PL, and Raman spectroscopy) on both doped and undoped compounds. We find that while the resistivity of Ti-, V-, Fe-, and Ni-doped ZnO decrease as compared to undoped ZnO, for Co, Cr, and Mn doping there has been an increase in the case of bulk polycrystalline samples. Similar to the undoped compound the ρ-T behavior of TM ion doped samples follow the Arrhenius conduction mechanism as well as 3D-VRH in higher- and lower-temperature regions, respectively, however the temperature range is different in each case. The decrease in resistivity to isovalent TM ion doped ZnO samples is attributed to the *d*-band splitting of the TM ion in the parent ZnO lattice. No ferromagnetism is detected in the doped bulk ZnO samples. Ti-, V-, Ni-, Cr-, Co-, and Mn-doped samples were paramagnetic in the measured temperature range (5–500K). However, Fe-doped samples exhibited a cusp at 12 K indicating the presence of an antiferromagnetic Néel temperature.

[1] Shubra Singh, P. Thiyagarajan, K. Mohan Kant, D. Anita, S. Thirupathiah, N. Rama, Brajesh Tiwari, M. Kottaisamy, and M. S. Ramachandra Rao, J. Phys. D **40**, 6312 (2007).

[2] Y. Natsume, H. Sakata, and T. Hirayama, Phys. Status Solidi A **148** 485 (1995).

[3] T. Dietl, H. Ohno, F. Matsukura, J. Cibert, and D. Ferrand, Science **287**, 1019 (2000).

[4] R. Triboulet and J. Perrière, Prog. Cryst. Growth Charact. Mater. **47**, 65 (2003).

[5] T. Makino, Y. Segawa, S. Yoshida, A. Tsukazaki, A. Ohtomo, and M. Kawasaki, Appl. Phys. Lett. **85**, 759 (2004).

[6] A. Segura, J. A. Sans, D. Errandonea, D. Martinez-García, and V. Fages, Appl. Phys. Lett. **88**, 011910 (2006).

[7] J. Zhong, S. Muthukumar, Y. Chen, Y. Lu, H. M. Ng, W. Jiang, and E. L. Garfunkel, Appl. Phys. Lett. **83**, 3401 (2003).

[8] C. Xu, M. Kim, J. Chun, and D. Kim, Appl. Phys. Lett. **86**, 133107 (2005).

[9] J. B. Cui and U. J. Gibson, Appl. Phys. Lett. **87**, 133108 (2005).

[10] Q. H. Li, Q. Wan, Y. G. Wang, and T. H. Wang, Appl. Phys. Lett. **86**, 263101 (2005).

[11] M. Lorenz, E. M. Kaidashev, A. Rahm, T. Nobis, J. Lenzner, G. Wagner, D. Spemann, H. Hochmuth, and M. Grundmann, Appl. Phys. Lett. **86**, 143113 (2005).

[12] K. Sato and H. Katayama-Yoshida, Physica B **308-310**, 904 (2001).

[13] K. Ueda, H. Tabota, and T. Kamai, Appl. Phys. Lett. **79**, 988 (2001).

[14] N. H. Hong, J. Sakai, and A. Hassini, J. Phys.: Condens. Matter **17**, 199 (2005).

[15] T. Wakano, N. Fujimura, Y. Morinaga, N. Abe, A. Ashida, and T. Ito, Physica E (Amsterdam) **10** 260 (2001).

[16] Shubra Singh, N. Rama, and M. S. Ramachandra Rao, Appl. Phys. Lett. **88**, 222111 (2006).

[17] H. Katayama-Yoshida and K. Sato, Physica B **327**, 337 (2003).

[18] W. Jung, S. J. An, G. C. Yi, C. U. Jung, S. I. Lee, and S. Cho, Appl. Phys. Lett. **80**, 4561 (2002).

[19] H. Hecht, in *Modern Aspects of Reflectance Spectroscopy*, edited by W. Wendlandt (Plenum, New York, 1968), pp. 1–22.

[20] P. Koidl, Phys. Rev. B **15**, 2493 (1977).

[21] A. M. Becerra and A. E. Castro-Luna, J. Chil. Chem. Soc. **50**, 465 (2005).

[22] A. Tuel, I. Arcon, and J. M. M. Millet, J. Chem. Soc., Faraday Trans. **94**, 3501 (1998).

[23] T. Grygar, J. Dedecek, P. P. Kruiver, M. J. Dekkers, P. Bezdicka, and O. Schneeweiss, Catena **53**, 115 (2003).

[24] H. Saeki, H. Tabata, and T. Kawai, Solid State Commun. **120**, 439 (2001).

[25] C. H. Bates, W. B. White, and R. Roy, J. Inorg. Nucl. Chem. **28**, 397 (1966).

[26] M. Jakani, G. Campet, J. Claverie, D. Fichou, J. Pouliquen, and J. Kossanyi, J. Solid State Chem. **56**, 269 (1985).

[27] M. Godlewski, Solid State Commun. **47**, 811 (1983).

[28] M. Godlewski and M. Skowronski, Phys. Rev. B **32**, 4007 (1985).
[29] Y. F. Lu, H. Q. Ni, and Z. M. Ren, J. Appl. Phys. **88**, 498 (2000).
[30] N. Ashkenov, B. N. Mbenkum, C. Bundesmann, V. Riede, M. Lorenz, D. Spemann, E. M. Kaidashev, A. Kasic, M. Schubert, M. Grundmann, G. Wagner, H. Neumann, V. Darakchieva, H. Arwin, and B. Monemar, J. Appl. Phys. **93**, 126 (2003).
[31] J. Serrano, A. H. Romero, F. J. Manjo'n, R. Lauck, M. Cardona, and A. Rubio, Phys. Rev. B **69**, 094306 (2004).
[32] F. J. Manjón, K. Syassen, and R. Lauck, High Press. Res. **22**, 299 (2002).
[33] F. J. Manjon, B. Marí, J. Serrano, and A. H. Romero, J. Appl. Phys. **97**, 053516 (2005).
[34] M. Rajalakshmi, A. K. Arora, B. S. Bendre, and S. Mahamuni, J. Appl. Phys. **87**, 2445 (2000).
[35] J. M. Calleja and M. Cardona, Phys. Rev. B **16**, 3753 (1977).
[36] Y. H. Yang, C. X. Wang, B. Wang, Z. Y. Li, J. Chen, D. H. Chen, N. S. Xu, G. W. Yang, and J. B. Xu, Appl. Phys. Lett. **87**, 183109 (2005).
[37] A. Kaschner, U. Haboeck, M. Strassburg, M. Strassburg, G. Kaczmarczyk, A. Hoffmann, C. Thomsen, A. Zeuner, H. R. Alves, D. M. Hofmann, and B. K. Meyer, Appl. Phys. Lett. **80**, 1909 (2002).
[38] C. Bundesmann, N. Ashkenov, M. Schubert, D. Spemann, T. Butz, E. M. Kaidashev, M. Lorenz, and M. Grundmann, Appl. Phys. Lett. **83**, 1974 (2003).
[39] J. D. Ye, S. L. Gu, S. M. Zhu, S. M. Liu, Y. D. Zheng, R. Zhang, Y. Shi, Q. Chen, H. Q. Yu, and Y. D. Ye, Appl. Phys. Lett. **88**, 101905 (2006).
[40] S. Bandyopadhyay, G. K. Paul, R. Roy, S. K. Sen, and S. Sen, Mater. Chem. Phys. **74**, 83 (2002).
[41] Shubra Singh, N. Rama, K. Sethupathi, and M. S. Ramachandra Rao, J. Appl. Phys. **103**, 07D108 (2008).
[42] K. Sato and H. Katayama-Yoshida, Phys. Status Solidi B **229**, 673 (2002).
[43] J. H. Park, M. G. Kim, H. M. Jang, S. Ryu, and Y. M. Kim, Appl. Phys. Lett. **84**, 1338 (2004).
[44] E. Badaeva, Y. Feng, Daniel R. Gamelin, and Xiaosong Li, New J. Phys. **10**, 055013 (2008).
[45] S. C. Wi, J.-S. Kang, J. H. Kim, S.-B. Cho, B. J. Kim, S. Yoon, B. J. Suh, S. W. Han, K. H. Kim, K. J. Kim, B. S. Kim, H. J. Song, H. J. Shin, J. H. Shim, and B. I. Min, Appl. Phys. Lett. **84**, 4233 (2004).
[46] M. Kobayashi, Y. Ishida, J. l. Hwang, T. Mizokawa, A. Fujimori, K. Mamiya, J. Okamoto, Y. Takeda, T. Okane, Y. Saitoh, Y. Muramatsu, A. Tanaka, H. Saeki, H. Tabata, and T. Kawai, Phys. Rev. B **72**, 201201(R) (2005).
[47] Rajesh Kumar and Neeraj Khare, Thin Solid Films **516**, 1302 (2008).
[48] L. Yan, C. K. Ong, and X. S. Rao, J. Appl. Phys. **96**, 508 (2004).
[49] J. Han, P. Q. Mantas, and A. M. R. Senos, J. Eur. Ceram. Soc. **22**, 49 (2002).
[50] K. Tominaga, T. Takaoa, A. Fukushima, T. Morigab, and I. Nakabayashib, Vacuum **66**, 511 (2002).
[51] G. Cao, S. McCall, J. Bolivar, M. Shepard, F. Freibert, P. Henning, J. E. Crow, and T. Yuen, Phys. Rev. B **54**, 15144 (1996).
[52] S. Ramachandran, Ashutosh Tiwari, and J. Narayan, Appl. Phys. Lett. **84**, 5255 (2004).
[53] D. Shimono, S. Tanaka, T. Torikai, T. Watari, and M. Murano, J. Ceram. Proc. Res. **2**, 184 (2001).
[54] J. H. He, C. S. Lao, L. J. Chen, D. Davidovic, and Z. L. Wang, J. Am. Chem. Soc. **127**, 16376 (2005).
[55] Yang-Ming Lu, Shu-I Tsai, and Chen-Min Chang, MRS Symposium Proceedings No. H10.11 (Materials Research Society, Pittsburgh, 2007).
[56] Y. R. Park and K. J. Kim, Solid State Commun. **123**, 147 (2002).
[57] W. Gebicki, K. Osuch, C. Jastrzebski, Z. Golacki, and M. Godlewski, Superlattices Microstruct. **38**, 428 (2005).
[58] S.-S. Lin, J.-L. Huang, and D.-F. Lii, Mater. Chem. Phys. **90**, 22 (2005).